J. Chem Soc. Nigeria, Vol. 44, No. 6, pp 1095 -1105 [2019]

COMPUTATIONAL MODELLING OF THE KINETIC AND THERMODYNAMIC STUDIES OF DIELS-ALDER REACTION OF ACROLEIN AND 1, 3-BUTADIENE

O. O. Adeboye

Department of Chemistry, Emmanuel Alayande College of Education, Oyo. Nigeria

Corresponding author's email: moadeb5848@yahoo.com Tel: +2348058484417

Received 16 August 2019; accepted 19 September 2019, published online 25 October 2019

ABSTRACT

The kinetics and thermodynamics of the Diels-Alder reaction of acrolein and 1, 3-butadiene to produce 3-cyclohexenecarboxaldehyde (1,2,3,6-Tetrahydrobenzaldehyde), a fragrance and masking ingredient used in many skin care products was modelled in the gas-phase using Density Functional Theory (DFT) at B3LYP level with 6-311++G (2df, 2P) basis set. Geometric parameters such as bond length, bond angle and dihedral angle, atomic charge distribution for the reactant (GS), transition state (TS) and the product (PRD) were obtained, kinetic and thermodynamic parameters were calculated. The reaction proceeded through a concerted asynchronous six-membered cyclic transition state. Bond breaking as shown by the values obtained for the change in the bond length between the transition state and the reactants (Δd) for [C_1 –C_5 = + 0.03Å, C_3-C_8 = +0.054 Å and C_4-C_{11}= +0.058 Å] occurred first while the bond making process is lagging behind in a single step, with values [C_1 –C_3 = - 0.06 Å, C_3-C_{11} = -2.301 Å and C_5-C_{14}= -1.514 Å] lower, compared with the values for bond breaking. This showed the concertedness and asynchronicity of the reaction. Electrostatic potential maps, LUMO maps, local ionization potential maps and HOMO-LUMO maps perfectly explain the molecular charge distribution. The kinetic [ΔH^*= 73.290 kJ/mol, ΔG^*=80.766kJ/mol, E_a =78.472kJ/mol, Rate, k =8.41 x 10^5] and thermodynamic [$\Delta H_{reaction}$ = -145.945 kJ/mol, $\Delta S_{reaction}$= -29.867J/mol.K, $\Delta G_{reaction}$ = -127.255 kJ/mol] values with the Arrhenius plots which resulted in a negatively sloped line with a steeper slope, showed that the activation energy is higher, this means that the reaction changes more rapidly and the rate constant is inversely proportional to the temperature. Negative values obtained for the enthalpy of reaction and Gibb's free energy showed that the reaction is exothermic and spontaneous respectively, energy of formation obtained confirms the exothermicity of the reaction as stated by Hammond's postulate. The plot of rate constant, k versus temperature showed that increase in temperature increases the rate constant and the plot of (1/T versus ln k) showed that as the temperature increases the rate constant decreases.

Keywords: Diels Alder reaction, Acrolein, 1, 3-butadiene, modelling

1.0 INTRODUCTION

Chemistry world has been encouraged to develop new chemistry that are less hazardous to human health and environment, less expensive and not time consuming (Anastas and Werner, 1998). Computational chemistry involves the use of principle of computer science to solve chemical problems. It uses the data obtained from theoretical calculations incorporated into efficient computer software to calculate the properties of molecules and solids. The properties includes position of the constituent atom, absolute and relative energies, electronic charge distributions, dipole, vibrational

frequencies reactivities, geometric parameters such as bond length, bond angle, dihedral angles and other spectroscopic quantities. Computational chemistry aimed at solving Schrodinger equations for electronic and nuclear motions using different functional such as Hartree Fock, Density Functional theory (DFT) and semi-empirical methods. It is a method that generate data to complement experimental data on structures, properties and reactions of substances (Shodor,1999-2000) Advancement in computational chemistry has allowed quantum mechanical calculations to support research in green chemistry and it has contributed immensely to the green nature of chemical practices. Computational chemistry allows for the testing of the toxicity of chemicals through the means that do not involve human or animal subject (Mazzali *et al*., 2009). Computational chemistry has entered into all areas of research some of the areas of interest are drug discovery, drug designing (Adejoro *et al*., 2016, Adejoro *et al*., 2017); Philomena, 2017 in her study on computational modeling in heterogeneous catalysis showed that DFT has strongly contributed to gather mechanistic insights and to develop universally valid conceptual frame works, such as the BEP relations based on DFT-based adsorption energies and reaction of molecules at catalyst surfaces, structure, bonding and reactivities. Computational modeling has been used to study molecular structure and vibrational spectra (Yunusa and Sahar, 2015), various pyrolytic reactions, Diels-Alder reaction (the mechanisms, kinetics and thermodynamics) in the gas-phase (Doering *et al.*, 1988, Chuan-Ming *et al.*, 2013, Adeboye, 2017, Adeboye, 2018, Adeboye *et al.*, 2018).

Diels-Alder reactions occurs when α, β unsaturared carbonyl undergo reaction with conjugated diene (Figure 1). They are reactions of type [4+2] cycloaddition reaction which involves molecules with conjugated π-system (a diene) and another with at least a π-bond (a dienophile), that is the 4 π electrons of the conjugated diene and the 2 π electrons of the dienophile (Morrison and Boyd, 2002, Anslyn and Dougherty 2006). Diels Alder reactions are important cycloaddition reaction and the most important pericyclic reaction; they are extensively used in carbon-carbon bond and ring formation. The study of Diels-Alder reaction has attracted interest because of its importance in the synthesis of diene, it is also used in the synthesis of new organic compounds through a six-membered cyclic system (Balbi and Khoumeri, 1994; Boger, 1991; Li and Houk, 1993; Celius, 2010; Aswany *et al*., 2016).

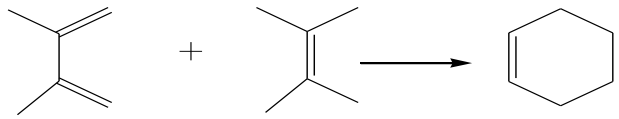

Diene Dienophile Cyclo-product

Figure 1: Diels-Alder reaction

However, there are limited works explaining the place of computational quantum modeling especially in the area of kinetic and thermodynamic study of chemical reactions. Therefore this work presented the computational modeling of the kinetic and thermodynamic parameters of Diels-Alder reaction of acrolein and 1, 3-butadiene in the gas-phase to produce 3-cyclohexenecarboxaldehyde, a fragrance and masking ingredient used in many skin care products in a way to enhance the principle and practice of chemistry to reduce the release of hazardous chemicals to the environment.

2.0 Computational Methodology

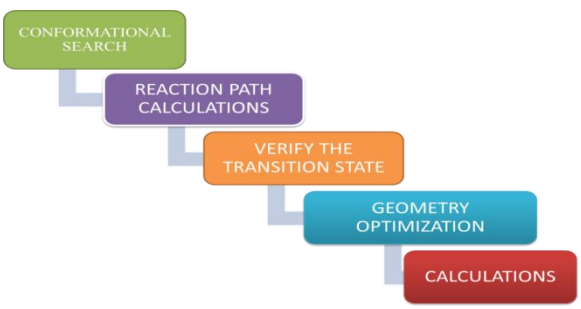

Figure 2: Graphical illustration of computational methodology

Conformational search (Hehre, 2003) was done on the reactants using molecular mechanics force field (MMFF) to obtain the reactants that has the lowest energy which is an indication of the stability of the reactants. Reaction path calculations were carried out using C_5-C_{14} and C_8 -C_{11} as the reaction coordinate this was done by slowly altering the bond distance between C_5-C_{14} and C_8 -C_{11} (4.168 Å and 4.343 Å) to the normal (1.543 Å and 1.534Å) bond length in the product form in 20 iterations. This was done to obtain the mechanism of the reaction. Optimization was performed on the transition state structure to obtain the true transition state; this was subjected to tests to verify that the transition state structure has only one imaginary vibrational frequency (IR value) and that the saddle point connects the ground state, transition state and product together. The intrinsic reaction coordinates method was also used by optimizing the molecule subject to a fixed position along the reaction coordinate (Warren and Sean, 2010). Full geometry optimization was then carried out on the structure of the reactants(GS), the transition states(TS) and products (PRD) to obtain the geometric parameters such as bond lengths, bond angles, dihedrals and atomic charges. Kinetics and thermodynamic calculations was done to obtain the kinetic and thermodynamic parameters using Density Functional Theory (DFT) at B3LYP level with 6-311++G (2df, 2P) basis set in Spartan' 10 version 1.0.1. (Deppmeier *et al.*, 2010)

3.0 RESULTS AND DISCUSSION

3.1 Conformational Search

Conformational search using molecular mechanics force field (MMFF) with systematic algorithm showed that there are four different conformers (Figure 3) with figure I having the lowest energy value of 48.57kJ/mol.

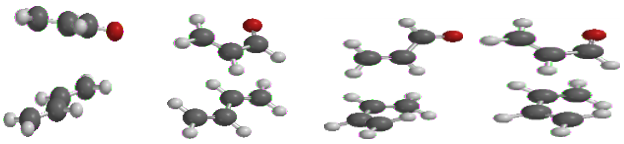

I=48.57kJ/mol II= 56.95 kJ/mol III=62.44 kJ/mol IV= 67.30 kJ/mol

Figure 3: Structures of the different conformers

3.2 Reaction Mechanism

The reaction (Figure 4) proceeds through a concerted asynchronous six-membered cyclic transition state which involves the transfer of electron (breaking of bonds) from three different π-bonds (C_1= C_5, C_3= C_8 and C_{11}= C_{14}) and the formation of one new π-bond between $C_1 - C_3$ and two new σ-bonds between $C_8 - C_{11}$ and $C_5 - C_{14}$. The true saddle point was characterized and verify by the presence of only one imaginary vibrational frequency (IR= i435cm^{-1}) which smoothly connect the reactant, the transition state and the product together. Asynchronicity was determined by the change bond length of the transition state and the corresponding reactant, for a reaction to be totally synchronous, the value must be zero. Table 1 showed that Δd= +0.03 Å, +0.054 Å and +0.058 Å for bond breaking and -0.06 Å, -2.301 Å and -1.514 Å for the bond formation respectively, an indication that the breaking of bond occurs first while the bond formation is lagging behind.

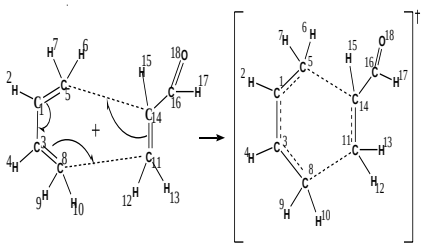

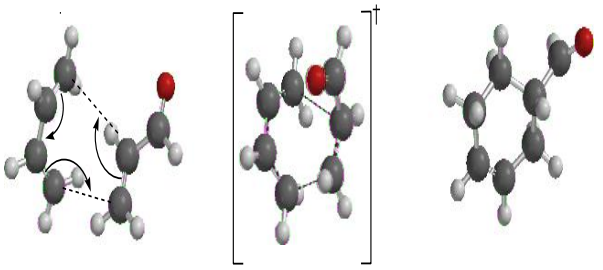

REACTANTS TRANSITION STATE PRODUCT

Figure 4: Reaction mechanism of Diels-Alder reaction of 1, 3-butadiene and acrolein

The reaction mechanism was also analyzed using the bond density surface (Figure 5) of the reactant, transition state and the product, the breaking between $C_1 – C_5$ and C_1 - C_3 internal rearrangement, not that prominent and formation of bonds between C_8- C_{11} and C_5 - C_{14} is so clear in the transition state . It is also obvious that the transition state structure resembles the reactants more closely than that of the products as obvious from the value of the energy of formation of transition state (GS=-913462.047kJ/mol, TS= -913392.468 kJ/mol and Product= -913645.891 kJ/mol) closer to the energy of formation of the reactant and thus confirming the exothermicity of the reaction as reported literature (Morrison and Boyd, 2002).

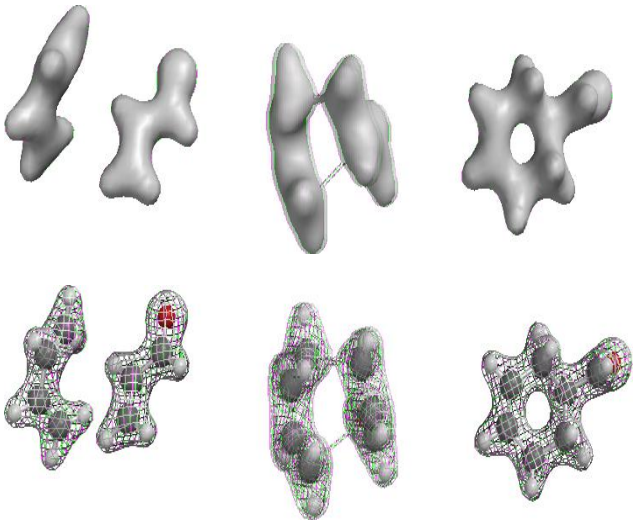

Figure 5: Bond density surface for the reactant, transition state and the product

3.3 Geometry optimization

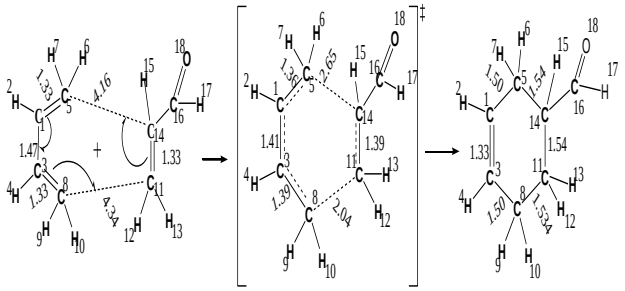

1, 3-butadiene + Acrolein 3-Cyclohexenecarboxaldehyde

Reactants **Transition state** **Product**

Figure 6: Optimized geometry of the reactants, transition state and products

Geometry optimization (Figure 6) was done on the reactants, the transition states and the products to obtain the geometric parameters such as bond length (Table 1). The values obtained were used to analyze the process of bond breaking and bond formation. The reaction was initiated from the diene (electron rich system) (Figure 2) as observed in the release of electron from C_1= C_5 to C_1= C_3, from C_3= C_8 to C_8- C_{11} and from C_{11}= C_{14} to C_5 – C_{14}. The bond length between C_1= C_5 in the reactant state is 1.336 Å, in the transition state the value has increased to 1.366 Å due to a kind of stretching involved in the breaking of bonds showing that the double bond is about to assume the form of a single bond which finally emerged at the product state with value (1.507 Å) corresponding to the bond length of a carbon- carbon single bond. C_1= C_3 is observed assuming a double bond as shown in the trend of decreasing bond length from 1.470 Å, 1.410 Å and 1.332 Å for the reactant, transition and product state respectively. C_3- C_8 a double bond shows increase in the bond length value (1.336 Å, 1.390 Å and 1.506 Å) in the reactant, transition and also to finally assume a single bond in the product state. It becomes interesting to observe that between C_8/ C_{11} and C_5/ C_{14} no bonds exist in the reactant state, the atoms are far apart with wide distance of 4.343 Å and 4.168 Å respectively. The trend of the decrease

in the bond length from 4.343 Å, 2.042 Å and 1.544 Å; 4.168 Å, 2.654 Å, and 1.543 Å for the reactant state, transition state and product, expressly announce the formation of two new σ-bonds between C_8- C_{11} and C_5 – C_{14}. The variation observed in the bond angle (Table 2) and in the dihedral angle (Table 3) is as a result of the distortion that occurs during the breaking and the formation of new bonds.

Table 1: Bond Length (Å)

Bond	Ground State(GS)	Transition State(TS)	PRD	Δd=TS-GS
$C_1 – H_2$	1.085	1.086	1.088	+0.001
C_1 - C_3	1.470	1.410	1.332	-0.06
$C_3 – H_4$	1.085	1.086	1.088	+0.001
$C_1 – C_5$	1.336	1.366	1.507	+0.03
$C_3 – C_8$	1.336	1.390	1.506	+0.054
$C_8 – C_{11}$	-	2.042	1.534	-2.301
$C_{11} – C_{14}$	1.335	1.393	1.544	+0.058
$C_{14} – C_5$	-	2.654	1.543	-1.514
$C_{14} – C_{16}$	1.474	1.454	1.511	-0.02

Table 2: Bond Angle (º)

Bond Angle	Ground State (GS)	Transition State(TS)	Product
C_1- $C_3 – C_8$	125.99	122.60	123.38
C_3- $C_1 – C_5$	125.90	117.40	123.73
C_5- $C_1 – H_2$	118.44	118.38	116.63
C_3- $C_8 – H_9$	121.36	118.33	109.80
C_{14}- $C_{11} – H_{13}$	121.29	118.68	110.20
C_{11}- $C_{14} – C_{16}$	121.33	119.52	110.29

Table 3: Dihedral Angle (º)

Dihedral Angle	Ground State (GS)	Transition State(TS)	Product
C_5- C_1- $C_3 – C_8$	31.74	0.01	1.39
H_2- C_1- $C_3 – C_8$	-149.63	-168.60	-179.01
C_1- C_3- $C_8 – H_9$	-118.60	179.73	136.59
H_{15}- C_{14}- $C_{11} – H_3$	-179.88	11.97	62.50
C_{16}- C_4- $C_{11} – H_{12}$	179.97	-160.01	61.92

3.4 Atomic Charge Distribution

Atomic charge (Table 4) calculation is very important to molecular systems because it affect molecular properties like polarizability, dipole moment and electronic structures. Atomic charge was calculated in Mulliken charge distribution for the reactant, transition and product state (Figure 7). Higher values obtained for change in the atomic charge (Δq) on C_5, C_8 and C_{11} +0.635, +0.6683 and +0.665 facilitated the release of electrons for bond formation.

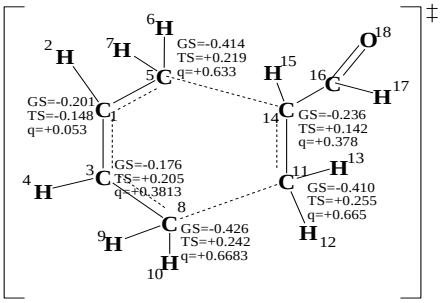

Figure 7: Atomic Charge Distribution shown on the transition state structure

Table 4: Atomic Charge Distribution

Atoms	Ground State (GS)	Transition State(TS)	Product	Δq=TS -GS
C_1	-0.201	-0.148	-0.171	+0.053
C_3	-0.176	+0.205	-0.163	+0.381
C_5	-0.414	+0.219	-0.405	+0.633
C_8	-0.426	+0.242	-0.428	+0.668
C_{11}	-0.410	+0.255	-0.422	+0.665
C_{14}	-0.236	+0.142	-0.310	+0.378
C_{16}	-0.093	+0.200	+0.150	+0.293

Electrostatic Potential map (Figure 8) charge distribution in a molecule provides deep insight into physical and chemical properties, charged molecules are water soluble. Positively charged site in a molecule invites attack by nucleophiles and negatively-charged sites are targeted by

electrophiles, a way to describe molecules charge distribution is to assign atomic charge for each atom but formal charges are arbitrary. A better alternative to describe molecular charge distribution is to use a quantity term electrostatic potential which is the energy interaction of a point positive charge with the nuclei and electron of a molecule. The point charge is placed in a region of excess positive charge which is the electron poor region, here the point charge-molecule interaction is repulsive and the electrostatic potential will be positive. On the other hand if the point charge is placed in a region of excess negative charge which is an electron rich region, the interaction is attractive and the electrostatic potential will be negative. Using the electrostatic potential map as mapped out using different colours. Red colour show the low energy end, (oxygen, carbon-carbon double bond in the dienophile) depict the region of most negative electrostatic potential and blue depicts the regions of most positive electrostatic (diene carbons) potentials. Electrostatic potentials increases is in the order of red< orange< yellow< green <blue. The colour reveals the overall charge distribution, the red region is the electron rich and the blue region is the electron poor, as can be seen in the values obtained for the change in charge distribution (Δq) between the reactant and the transition state (Table 4) for C_5 =+0.633, -0.066, C_8= +0.668, -0.074 C_{11} = +0.665. -0.046 mostly of the blue side and C_3 =+0.381, +0.067, C_{14} =+0.378, 0.032 and C_{16} =+0.107, +0.024 on the green side.

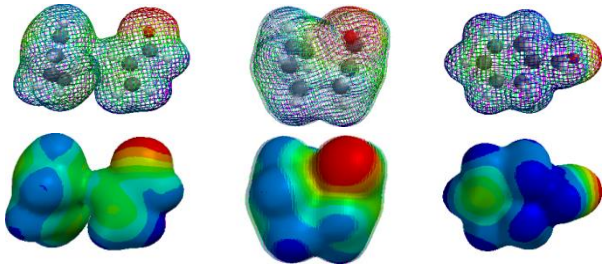

Figure 8: Electrostatic Potential map in mesh and solid form for the reactant, transition state and product

The LUMO map (Figure 9) mapped out the absolute value of the LUMO on an electron density surface as calculated for the reaction, transition and product state. This shows where electron pair (a nucleophile) might attack. The LUMO map shows which region of a molecule are most electron deficient, and hence most subject to nucleophilic attack, the position of attack is the blue region (electron loving region seeking electron) which has been shown in the calculation with affinity value (1.83 eV) lower compared with the red region electron rich site with ionization potential value (6.76eV) and as shown in the blue area, we have C_{11}=C_{14} of the dienophile , the two carbons are in α and β position to the functional group and are responsible for the formation of the two new σ-bond between C_8-C_{11} and C_5-C_{14}.

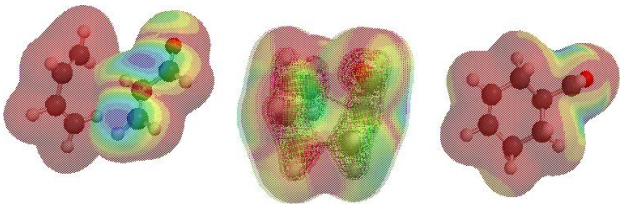

Figure 9: LUMO MAP for the reactant, transition state and product

The local ionization potential (Figure 10) provides a measure of the relative ease of electron removal (ionization) at any location around the molecule. The local ionization potential ($-E_{HOMO}$ eV) map is of great importance in that it reveals those regions from which electrons are most easily ionized (blue region) with high ionization potential (+6.75eV), it reveals the sites which are susceptible to electrophilic attack, the colour red area, mostly around the area of the C=C double bond in the reactant corresponds to regions of lowest (+1.83eV) ionization potential (affinity, $-E_{LUMO}$) that is most accessible to electrophiles. The diene is electron rich and the dienophile is seeking electron.

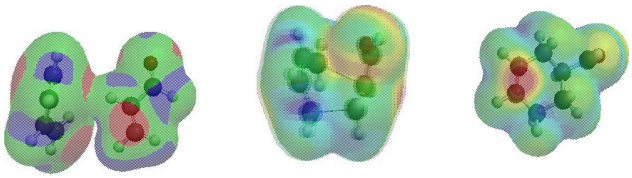

Figure 10: Local ionization potential for the reactants, transition state and product in solid form

3.5 Frontier Molecular Orbital Theory

Using Frontier Molecular Orbital theory (Figure 11) the highest occupied molecular orbital (HOMO) and lower unoccupied molecular orbitals (LUMO) are useful in analyzing the reactive position in the π-electron systems (Babu *et al*., 2011). Due to the energies of these orbitals being the closest of any orbitals to different energy levels, the HOMO-LUMO gap (Table 5) is where the most likely excitement can occur. Excitation is easier with converged HOMO-LUMO gap and the greater the mobility of the π- electron in the large conjugated Pi orbital system, the greater the distribution of the energy throughout the molecule (Truong-Son,2015 https://socratic.org/questions). Electron flow from the populated $\pi_{C=C}$ molecular orbital of one component into the vacant $\pi^*_{C=C}$ of the other component. (Anslyn and Dougherty, 2006). The energy of HOMO is related to the ability to donate (ionization potentials) electrons while the energy of the LUMO is related to the ability to accept electrons (electron affinity).

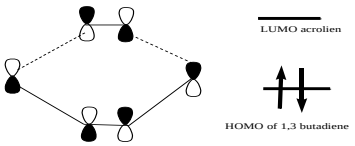

Figure 11: Frontier Molecular orbital theory analysis of cycloaddition reaction of the HOMO of 1, 3 butadiene and LUMO of acrolein

Considering the HOMO-LUMO map (Figure 12) the energy of LUMO is higher compared with the energy of HOMO that is HOMO (-6.75eV) is electron rich, the diene (red zone) and LUMO (-1.83 eV) electron loving, dienophile (blue zone) which is in line with literature that the common interaction for Diels Alder reaction is a [4+2] cycloaddition where the HOMO of the diene interact with the LUMO of the dienophile and as the two molecules approach each other, mixing between the filled and empty molecular orbitals has to stabilize, HOMO-LUMO mixing will be favourable because these orbitals have smaller energy gap (+4.92eV in the reactant), because the stabilizing interaction occurs as the reactants approach each other, this certainly persist in the transition state (+4.08eV) (Table 5) thereby favouring the reaction because valence electron in the HOMO can absorb lower energy to excitation of the electrons and this thus favoured the normal electron demand pull (Anslyn and Dougherty, 2006).

Table 5: HOMO-LUMO Energy Gap

Substituent	State	Homo (Ev)	Lumo (Ev)	E. Gap (Ev) (Lumo-Homo)
H	GS	-6.75	-1.83	+4.92
	TS	-6.14	-2.06	+4.08
	PRD	-6.87	-0.80	+6.07

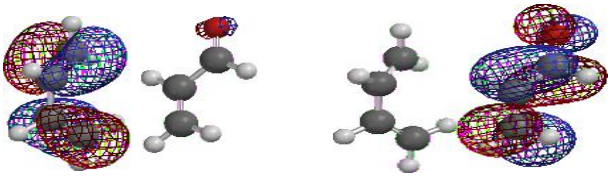

HOMO (-6.75eV) LUMO (-1.83 eV)

Figure 12: HOMO-LUMO MAP for the reactants (1,3 butadiene and acrolein)

3.6 Kinetic and Thermodynamic parameters at 623K

The negative values (Table 6) obtained for the enthalpy of reaction and Gibb's free energy values ΔH -145.945 kJ/mol and $\Delta G_{reaction}$ = -127.255 kJ/mol showed that the reaction is exothermic in agreement with submission that Diels-Alder reactions often takes place with evolution of heat when reactants simply mixed together (Morrison and Boyd, 2002)

and spontaneous (Anslyn and Dougherty, 2006) respectively.

The activation parameters ΔH* (73.290 kJ/mol), rate constant, k (8.41 x $10^5 mol^{-1}$ t^{-1}), Ea 78.472 kJ/mol and ΔG* 80.766 kJ/mol shows that that the reaction change more rapidly (Table 6). Negative entropy of activation obtained (-11.72 J/mol.K) is in agreement with the literature (Anslyn and Dougherty, 2006).

Table 6: Kinetic and Thermodynamic parameters at 623K

Parameters	**Result**
Energy of Formation	GS -913462.047 kJ/mol TS -913392.468 kJ/mol PRD-913645.891 kJ/mol
$\Delta H_{reaction}$	-145.945 kJ/mol
$\Delta S_{reaction}$	-29.867 J/mol.K
$\Delta G_{reaction}$	-127.255 kJ/mol
ΔS^*	-11.728 J/mol.K
K_{eq}	4.609 x10^{10}
log A	12.50
ΔH^*	73.290 kJ/mol
E_a	78.472 kJ/mol
Rate, k	8.41 x 10^5 M S^{-1}
ΔG*	80.766 kJ/mol

Increases exponentially. As the temperature increases in chemical reaction, the kinetic energy of the particle also increases making them to move faster, this increases the chance of collision and the rate of reaction.

Considering Figure 13a, as the temperature increases activation energy also increases and the slope steepees which means the activation energy is higher, this also means that the reaction change more rapidly. Figure 13b shows the variation of temperature with rate constant, k and according to literature (https://chem.libretexts.org>Bookshelves) if A, Ea and RT are constant the typical plot of rate constant versus T is as shown in the plot obtained below. The Arrhenius plot (Figure 13c) resulted in a negatively sloped line; this can be used to find other missing components of Arrhenius equations. From the plot, extrapolating the line back to the y-intercept gives the pre-exponential factor A, which is approximately 28.78 $M^{-1}s^{-1}$. The slope of the line gives the negative activation energy divided by R (-Ea/R) which is equal to -15.175.

Table 7 shows the variation of reaction rates with temperature as the temperature increases, rate

Temp (K)	**1/T (k)**	**ΔS* (J/mol.K)**	**A** ($M^{-1}s^{-1}$)	**RT** ($Jmol^{-1}$)	**Ea (kJ/mol)**	**K** (M S^{-1})	**ln k**
298	0.0034	-24.56	3.238E11	2.479	75.77	0.017	-4.07
323	0.0031	-22.73	4.373E11	2.687	75.98	0.22	-1.51
348	0.0029	-21.38	5.543E11	2.949	76.24	3.2	1.16
373	0.0027	-20.19	6.854E11	3.103	76.39	13	2.56
398	0.0025	-19.03	8.409E11	3.310	76.6	14	4.3
423	0.0024	-17.86	1.029E12	3.519	76.81	341	5.83
448	0.0022	-16.85	1.230E12	3.727	77.02	1300	7.17
473	0.0021	-15.98	1.442E12	3.935	77.23	4320	8.37
498	0.0021	-14.71	1.769E12	4.143	77.43	13500	9.51
523	0.0019	-14.02	2.019E12	4.351	77.64	35900	10.49
548	0.0018	-13.36	2.289E12	4.559	77.85	87800	11.38
573	0.0017	-12.71	2.585E12	4.767	78.06	200000	12.3
598	0.0017	-12.08	2.915E12	4.975	78.27	429000	12.97
623	0.0016	-11.73	3.167E12	5.183	78.47	841000	13.64

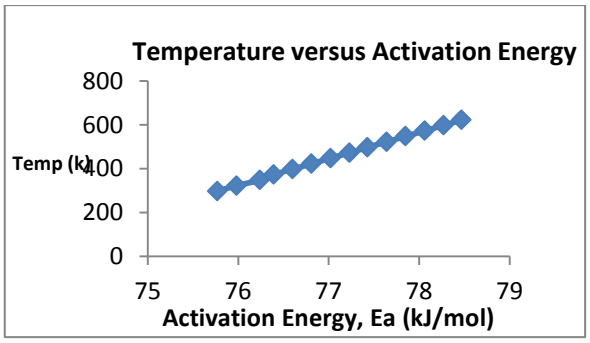

(a)

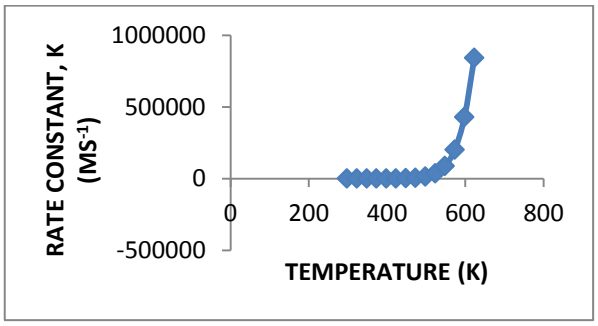

(b)

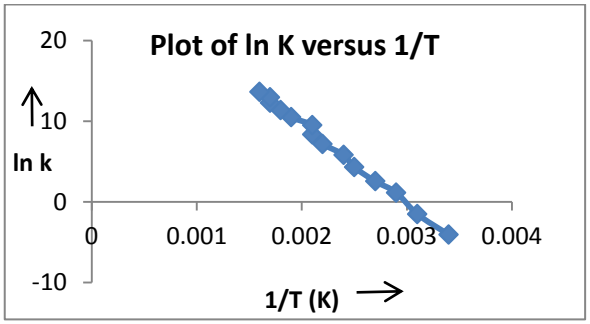

(c)

Figure 13 a, b & c: Plot showing the variation of temperature against (a) activation energy (kJ/mol) (b) rate constant, k (M/S) and (c) plot of ln k versus 1/T (kelvin)

4.0 CONCLUSION

This study presented the computational modeling study of the kinetics and thermodynamics of Diels Alder reaction of 1,3 butadiene and acrolein in the gas-phase using DFT at B3LYP level with 6-311++G(2df, 2p) basis set to promote the sustainability of green chemistry that is practice of chemistry to reduce the use of products, by-products, solvents or reagents that are hazardous to the environment. The result obtained for reaction mechanism, geometric parameters such as bond lengths, bond angles and dihedral angles for the reactants, transition state and product, values obtained for atomic charge and charge distribution to analyze parameters such as LUMO map, local ionization density map, electrostatic potential map charge distribution, local ionization potential map, frontier molecular orbital theory and HOMO-LUMO map and the values obtained for kinetic and thermodynamic parameters are true reflections of facts reported in literature (Warren, 2003; Anslyn and Dougherty, 2006). This is an indication that computational modeling is an environmentally friendly methodology because it helps researchers to get insight into the reaction mechanism, rate of reactions, quantity of heat required etc. This fore-knowledge helps to reduce cost, time of laboratory experiments and most importantly the level of exposure to and release of hazardous chemicals.

5.0 REFRENCES

[1] P. T. Anastas and J. C. Werner, (1998). Green Chemistry Theory and Practice, Oxford Science Publications, Oxford.

[2] T. Mazzali, AmyMoin, A. Paoquette, (2009). Analysis of Green Chemistry and Computational toxicology, EPA.

[3] SHODOR (1999- 2000). The Shodor Educational Foundation, Inc in cooperation with the National Center for Supercomputing Applications.

[4] I. A. Adejoro., S.O Waheed and O.O. Adeboye (2016). Molecular Docking Studies of *Lonchocarpus cyanescens* Triterpenoids as Inhibitors for Malaria. ***Journal of Physical Chemistry & Biophysics* 6: 213 1- 4 doi: 10.4172/2161 0398.1000213.**

[5] I. A. Adejoro, S. O. Waheed O. O. Adeboye, F. U. Akhigbe (2017). Molecular Docking of the Inhibitory Activities of Triterpenoids of *Lonchocharpus cyanescens* against Ulcer. ***Journal of Biophysical Chemistry:* 8, 1-11. https://doi.org/10.4236/jbpc.2017.81001.**

[6] P. Schlexer (2017). Computational Modeling in Heterogenous Catalysis Elsevier DOI: 10.1016/B978-0-12-409547-2.14273-8

[7] Y. Umar and S. Abdalla (2015). Experimental FTIR and Theoretical Investigation of the Molecular Sturcture and Vibrational Spectra of Terephthaloyl Chloride by Density Functional Theory ***IOSR Journal of Applied Chemistry (IOSR-JAC)*** 8 (9) 26-34.

[8] W.V.E Doering, W.R Roth, R. Breuckman, L Figge, H. W. Lennartz, W. D. Fessner, and H. Prinzbach, (1988). Diels Alder reaction: an assessment of quantum chemical procedures Journal of Chemical Physics 106 8727. http://doi.org/10.1063/1.473933.

[9] Chuan-Ming Wang, Yi-Lei Chen, Zhi-Hua Liu, Yong-Kuan Chien, Jing-Mei Han, Ming-Ming Miao and HuaiCao (2014). Theoretical Study on Synthesis of Sylvestrene by Cyclodimerization of Isoprene: Asynchronous Concerted Mechanism of Diels-Alder Reaction. ***Asian Journal of Chemistry*** 26(4) 1019-1026.

[10] O. O. Adeboye (2017). Computational Modelling of the Mechanisms, Kinetics and Thermodynamics of Pyrolysis of Isobutyl Bromide in the Gas-Phase**.** ***Chemical Science International Journal:* 18(4) 1-9.**

[11] O. O. Adeboye (2018). The Mechanisms, Kinetics and Thermodynamics of Gas-Phase Pyrolysis of *sec*-Butyl Bromide: A ComputationalApproach. ***International Journal of Pure and Applied Chemistry 16 (1) 1-10.***

[12] O. O. Adeboye, I. A. Adejoro, & A. M. Olatunde, (2018). Computational Modelling of the Kinetics and Thermodynamics of Diels-Alder reaction: 1,3-cyclohexadiene and substituted ethene. ***Leonardo Electronic Journal of Practices and Technologies 33, July-December 207-218.***

[13] R. T. Morrisson and R. N. Boyd, (2002). Organic Chemistry (Sixth Edition) Prentice-Hall of India Private Limited,New Delhi-110015.

[14] E. V. Anslyn, and D. A Dougherty (2006). Modern Physical Organic Chemistry. University Science books www.uscibooks.com

[15] N. Balbi, and B. Khoumeri, (1994). Thermodynamic and Kinetic studies on reversible liquid-phase Diels-Alder reaction between maleic anhydride and 2-methyl furan. Dynamic modelling by thermal analysis. ***Journal of Thermal Analysis***. 42 461-466.

[16] D. L. Boger, (1991). In HeteroDiene Additions: Trost, B. M.Ed, Pergamon Press: Oxford Vol.5 p. 451.

[17] Y. Li, and K.N. Houk (1993). Diels-Alder dimerization of 1,3-butadiene: An ab-initio CASSCF study of the concerted and stepwise mechanisms and butadiene-ethylene revisited, ***J. Am. Chem Soc.*** 115 7478- 7485.

[18] T. C. Celius, (2010). Fast Hetero-Diels-Alder Reactions using 4-Phenyl-1,2,4-triazoline-3,5-dione (PTAD) as the Dienophile. ***J. Chem Educ***. 87

[19] P.N Aswany, Arya Suresh, G. Vijayakumar, and T Renjith, (2016). Substituent effects on simple Diels-Alder reaction from Quantum Mechanical calculations. ***International Journal of Current Research in Chemistry and Pharmaceutical Sciences.*** (3) 5 40-47.

[20] W. J. Hehre 2003 A guide to Molecular Mechanics and Quantum Chemical Calculations Wavefunction, Inc. Irvine, CA 92612.

[21] W. Hehre and S. Ohlinger (2010). Spartan User guide for Windows, Machintosh and Linux. Wavefunction. Inc USA. 45.

[22] B. J. Deppmeier, A. J. Driessen, T. S. Hehre, W. J. Hehre, J. A. Johnson, P. E. Klunzinger, J. M. Leonard, I. N. Pham W. J. Pietro, JianguoYu (2010). Wavefunction Developers

[23] K. M., Babu, P. C., Sundaraganesan, N. Cinar and M. Karabacak, M. (2011). Molecular structure, vibrational, UV and NBO analysis of 4-chloro-7-nitrobenzofurazan by DFT calculations. ***Spectrochimica Acta Part A: Molecular and Biomolecular Spectroscopy***, 79 (5), 1162-1170.

[24] N.Truong-Son (2015). SOCRATIC https://socratic.org/questions. Chemistry>Bonding and Antibonding Orbitals.

[25] ChemistryLibreTexts – Temperature and Rate – Chemistry (https://chem.libretexts.org>Bookshelves)